AIP Applied Physics Letters

Strain-assisted current-induced magnetization reversal in magnetic tunnel junctions: A micromagnetic study with phase-field microelasticity

H. B. Huang, J. M. Hu, T. N. Yang, X. Q. Ma, and L. Q. Chen

Citation: Applied Physics Letters **105**, 122407 (2014); doi: 10.1063/1.4896692
View online: http://dx.doi.org/10.1063/1.4896692
View Table of Contents: http://scitation.aip.org/content/aip/journal/apl/105/12?ver=pdfcov
Published by the AIP Publishing

Articles you may be interested in
Simulation of electric-field and spin-transfer-torque induced magnetization switching in perpendicular magnetic tunnel junctions
J. Appl. Phys. **117**, 17A701 (2015); 10.1063/1.4906201

Magnetic tunnel junctions for magnetic field sensor by using CoFeB sensing layer capped with MgO film
J. Appl. Phys. **115**, 17E524 (2014); 10.1063/1.4868181

Electric field-induced magnetization reversal in a perpendicular-anisotropy CoFeB-MgO magnetic tunnel junction
Appl. Phys. Lett. **101**, 122403 (2012); 10.1063/1.4753816

Spin transfer switching in Tb Co Fe / Co Fe B / Mg O / Co Fe B / Tb Co Fe magnetic tunnel junctions with perpendicular magnetic anisotropy
J. Appl. Phys. **103**, 07A710 (2008); 10.1063/1.2838335

Estimation of spin transfer torque effect and thermal activation effect on magnetization reversal in Co Fe B / Mg O / Co Fe B magnetoresistive tunneling junctions
J. Appl. Phys. **101**, 09A511 (2007); 10.1063/1.2713695

This article is copyrighted as indicated in the article. Reuse of AIP content is subject to the terms at: http://scitation.aip.org/termsconditions. Downloaded to IP: 128.118.37.128 On: Thu, 05 Feb 2015 18:52:17

APPLIED PHYSICS LETTERS **105**, 122407 (2014)

Strain-assisted current-induced magnetization reversal in magnetic tunnel junctions: A micromagnetic study with phase-field microelasticity

H. B. Huang,[1,2,a),b)] J. M. Hu,[1,b)] T. N. Yang,[1] X. Q. Ma,[2] and L. Q. Chen[1]
[1]Department of Materials Science and Engineering, The Pennsylvania State University, University Park, Pennsylvania 16802, USA
[2]Department of Physics, University of Science and Technology Beijing, Beijing 100083, China

(Received 23 July 2014; accepted 16 September 2014; published online 25 September 2014)

Effect of substrate misfit strain on current-induced in-plane magnetization reversal in CoFeB-MgO based magnetic tunnel junctions is investigated by combining micromagnetic simulations with phase-field microelasticity theory. It is found that the critical current density for in-plane magnetization reversal decreases dramatically with an increasing substrate strain, since the effective elastic field can drag the magnetization to one of the four in-plane diagonal directions. A potential strain-assisted multilevel bit spin transfer magnetization switching device using substrate misfit strain is also proposed. © *2014 AIP Publishing LLC*. [http://dx.doi.org/10.1063/1.4896692]

Spin transfer torque (STT) effect[1,2] arises from the transfer of angular momentums from the electrons of the spin-polarized current to the local ferromagnet when a current goes through a spin-valve nanopillar. One of the most attractive applications is high density magnetic random access memory (MRAM),[3,4] which has the advantage of large storage density, high addressing speed, low energy consumption, and avoidance of cross writing. A memory cell of MRAM has two ferromagnetic layers separated by a nonmagnetic conductive spacer or thin insulating interlayer. One of two layers has a fixed magnetization along a predetermined direction, while the other magnetization of free layer could be reoriented by external magnetic field. Based on the STT effect, the magnetization reorientation can be induced by injecting a spin-polarized current into the free magnetic layer.[5–7] The current-induced switching eliminates crosstalk between neighboring cells during writing in using the external magnetic field.[8] Furthermore, STT-MRAM has practically unlimited endurance and requires less energy, and faster than conventional magnetic field control MRAM. However, the high critical switching current J_c of STT-MRAM has to be reduced for achieving the compatibility with the metal-oxide-semiconductor technology.

Many attempts have been made to reduce J_c. For example, using CoFeB as the free layer to reduce M_S;[9] using a double spin-filter structure,[10] an antiferromagnetic pinning structure,[11] or inserting a Ru spin scattering layer to increase spin scattering;[12] or using a composite free layer consisting of two ferromagnetic layers with various coupling types;[13–16] or using Heusler-based spin valve nanopillar.[17–23] Another possible approach to increasing the storage density is to store multiple bits per cell.[24–26] The combination of small critical current and multiple bits per cell in one device is the most desired path towards high density STT-MRAM. In magnetic thin films or islands, strain can be effectively utilized to tune the magnetic domain structures.[27–31] For example, the magnetization can be switched between an in-plane and out-of-plane orientation under isotropic biaxial in-plane strains,[32,33] or rotate within the film plane under anisotropic biaxial in-plane strains.[34] Recently, Pertsev and Kohlstedt[35] theoretically demonstrated that the critical current density needed for 180° magnetization switching in a free magnetic layer of spin valve can be reduced drastically by the assistance of substrate misfit strain. The conventional micromagnetic simulations do not take account of such effect of elastic energy and thus cannot be employed to investigate the assistance of substrate misfit strain in spin transfer magnetization switching.

In this work, we propose to combine the phase-field microelasticity theory with micromagnetic simulations to understand the effect of substrate misfit strain in spin transfer switching. In particular, we investigate strain-assisted spin transfer switching in CoFeB-based magnetic tunnel junctions. First, we show the strain distribution to illustrate the mechanism of strain-induced magnetization reorientation. Then, we discuss the effect of substrate strain assistance in spin transfer switching by showing magnetization trajectories and magnetic domain evolutions. At the end, we present a potential strain-assistance multilevel bit spin transfer magnetization switching by using substrate misfit strain.

We investigated spin-valve nanoislands with the structure of CoFeB (40 nm)/MgO (2 nm)/CoFeB (20 nm) of square cross section area as shown in Figure 1(a). We employed a Cartesian coordinate system where the current is along the z axis in Figure 1(b). The two CoFeB layers are separated by a thin MgO layer, and the bottom CoFeB layer is the free layer whose magnetization dynamics is triggered by a spin-polarized current. The top CoFeB layer is the pinned layer with its magnetization vector **P** fixed in the direction along the positive x axis. The initial magnetization vector **M** of the layer is along the negative or positive x axis. The free layer lateral length of spin valve magnetic island is fully constrained by a stiff substrate. We generally define the substrate strain represented by ε_{ii} (i = 1 and 2), and the positive current as electrons flowing from the free layer to the pinned layer. In this paper, the positive current will lead to the antiparallel structure (AP, "1") between the free layer and the pinned layer while the negative current will lead to the parallel structure (P, "0") according to the STT theory. To illustrate the mechanism of strain-assisted magnetization switching, Figure 1(c) shows the

a)Author to whom correspondence should be addressed. Electronic mail: houbinghuang@gmail.com.
b)H. B. Huang and J. M. Hu contributed equally to this work.

 © 2014 AIP Publishing LLC

This article is copyrighted as indicated in the article. Reuse of AIP content is subject to the terms at: http://scitation.aip.org/termsconditions. Downloaded to IP: 128.118.37.128 On: Thu, 05 Feb 2015 18:52:17

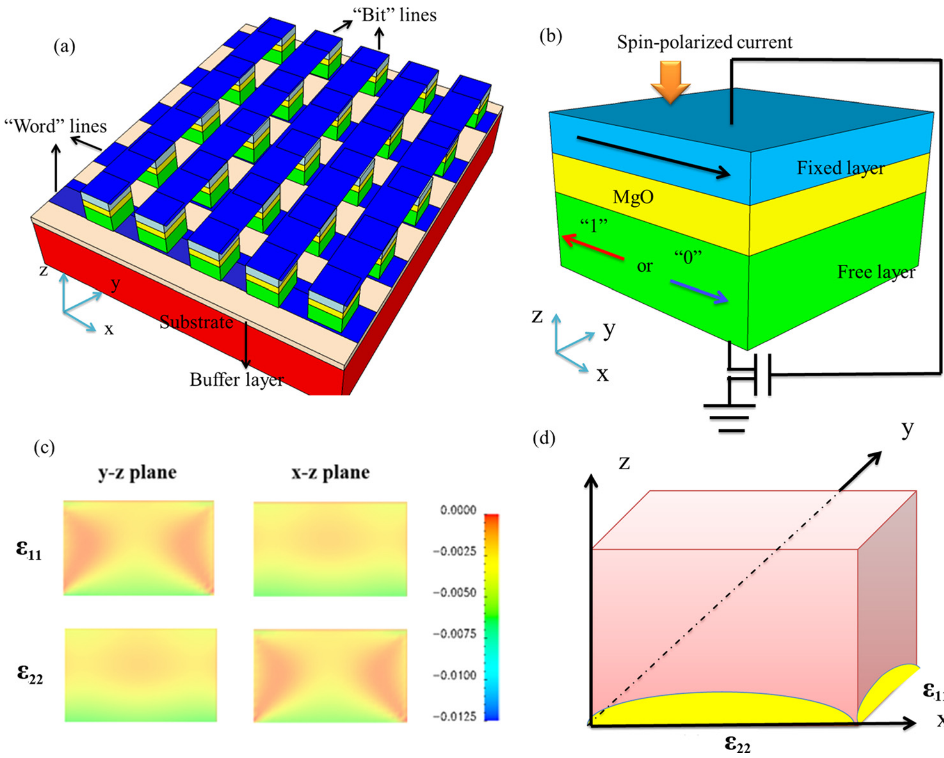

FIG. 1. Schematics of (a) the high density patterned bit array (b) the building block of CoFeB/MgO/CoFeB nanoisland spin valve in Cartesian coordinates. Spin-polarized current is applied perpendicularly to the island plane. (c) The strain distributions at different planes from phase-field simulations. (d) Illustration of strain distributions in 3D coordinate.

in-plane strain distributions ε_{11} and ε_{22} in the y-z and x-z planes under the condition of isotropic in-plane substrate strain $\varepsilon_{11} = \varepsilon_{22} = -0.9\%$. We observe that the largest strain is located in the interface of substrate, and the strain in the middle of nanoisland is larger than the strains in the corners. We use Figure 1(d) to illustrate the mechanical effect of substrate strain on the x-y plane. The strain will drag the magnetization from its initial direction (axial) to the four corner directions. Therefore, we can obtain 45° and 135° magnetization switching. Due to four possible diagonal directions, we can obtain four possible magnetization distributions which could be used in the multi-bit spin transfer magnetization switching.

The magnetization dynamics is described by using a generalized Landau-Lifshitz-Gilbert-Slonczewski (LLGS) equation[1,2]

$$\frac{d\mathbf{M}}{dt} = -\gamma'\mathbf{M}\times\mathbf{H}_{eff} - \frac{\alpha\gamma'}{M_s}\mathbf{M}\times(\mathbf{M}\times\mathbf{H}_{eff}) - \frac{2\mu_B J}{(1+\alpha^2)edM_s^3}g(\mathbf{M},\mathbf{P})\mathbf{M}\times(\mathbf{M}\times\mathbf{P}) + \frac{2\mu_B\alpha J}{(1+\alpha^2)edM_s^2}g(\mathbf{M},\mathbf{P})(\mathbf{M}\times\mathbf{P}), \quad (1)$$

where $\mathbf{H}_{\text{eff}}$ is the effective field, $\gamma' = \gamma/(1+\alpha^2)$, γ is the electron gyromagnetic ratio, and α is the dimensionless damping parameter. The effective field includes the anisotropy field, the demagnetization field, the external field, the elastic field, and the exchange field, namely, $\mathbf{H}_{\text{eff}} = \mathbf{H}_{\text{k}} + \mathbf{H}_{\text{d}} + \mathbf{H}_{\text{ext}} + \mathbf{H}_{\text{elas}} + \mathbf{H}_{\text{ex}}$, given as

$$\mathbf{H}_{eff} = -\frac{1}{\mu_0}\frac{\delta E}{\delta\mathbf{M}}, \quad (2)$$

where E is the total energy, expressed by $E = E_k + E_d + E_{ext} + E_{elas} + E_{ex}$, where E_k, E_d, E_{ext}, E_{elas}, and E_{ex} are anisotropy energy, demagnetization energy, Zeeman energy, elastic energy, and exchange energy, respectively. The details for obtaining E_k, E_d, E_{ext}, and E_{ex} can be found in our previous papers.[36–38] Note that a finite size magnet magnetostatic boundary condition[39] is applied to calculate the demagnetization energy E_d, to consider the influence of geometric size on the magnetic domain structures of such three-dimensional nanomagnets.

In particular, the elastic energy E_{elas} is calculated based on a previously developed phase-field model[40] for a three-phase system that is comprised of an isolated magnetic nanoisland (the free layer herein), a stiff substrate, and the air. In this case, the stress-free boundary condition at the top and lateral surfaces of the magnetic nanoisland can be automatically incorporated by setting the elastic constants of the air phase as zero. Overall, the integration of such phase-field model with micromagnetic simulations allows us to study the effect of the spatially variant strains [that are obtained after the mechanical relaxation of the substrate strain ε_{ii}, also see Fig. 1(d)] on the magnetic domain structure and magnetization dynamics. Mathematical expression and the detailed numerical solution of E_{elas} can be found in Ref. 40. The corresponding effective elastic field H_{elas} can be expressed as

$$\mathbf{H}^x_{\text{elas}} = \frac{2B_2^2 m_x m_z^2}{c_{44}} - 2B_1\varepsilon_{11}m_x,$$
$$\mathbf{H}^y_{\text{elas}} = \frac{2B_2^2 m_y m_z^2}{c_{44}} - 2B_1\varepsilon_{22}m_y,$$
$$\mathbf{H}^z_{\text{elas}} = \frac{2B_2^2 m_z(1-m_z^2)}{c_{44}} + 2B_1 \times \frac{\left[c_{12}(\varepsilon_{11}+\varepsilon_{22})m_z + 2B_1 m_z\left(m_z^2 - \frac{1}{3}\right)\right]}{c_{11}}, \quad (3)$$

where $B_1 = -1.5\lambda_{100}(c_{11}-c_{12})$ and $B_2 = -3\lambda_{111}c_{44}$, with λ_{100} and λ_{111} representing the magnetostrictive coefficients. From Eq. (3), it can be seen that the in-plane effective elastic field is

This article is copyrighted as indicated in the article. Reuse of AIP content is subject to the terms at: http://scitation.aip.org/termsconditions. Downloaded to IP: 128.118.37.128 On: Thu, 05 Feb 2015 18:52:17

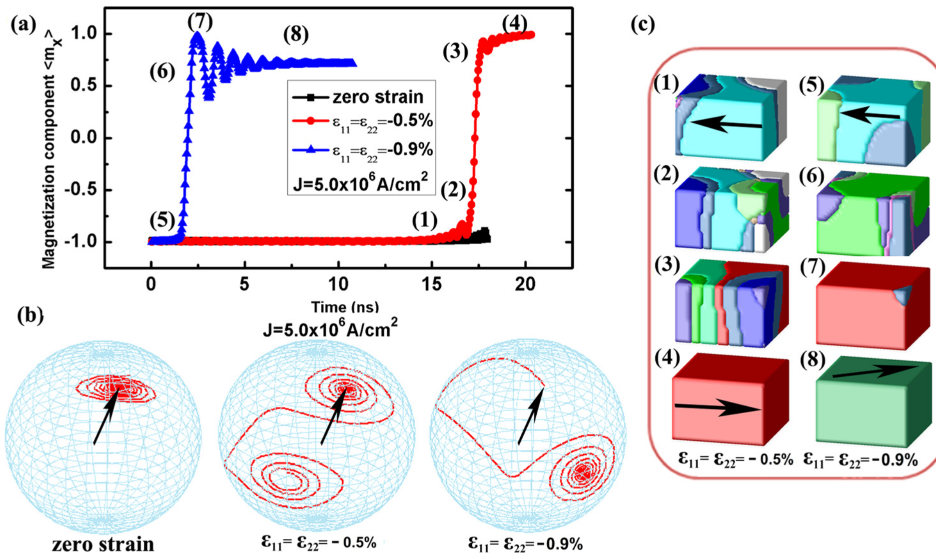

FIG. 2. (a) Temporal evolutions of the average normalized magnetization components $\langle \mathbf{m}_x \rangle$ with different substrate strains at the current density of 5.0×10^6 A/cm^2. (b) Magnetization trajectories at different strains. (c) Snapshots of magnetic domains evolution with different substrate strain at $J = 5.0 \times 10^6$ A/cm^2.

biaxial isotropic ($\mathbf{H}^x_{\text{elas}} = \mathbf{H}^y_{\text{elas}}$) under substrate-induced isotropic in-plane strains (i.e., $\varepsilon_{11} = \varepsilon_{22}$). In this case, the magnetization vector is likely to align along one of the four in-plane diagonal axes if not switching out of the film plane.[40]

The last two terms on the right side of Eq. (1) describe STT that tends to drag the magnetization away from its initial state to its final state. The scalar function is given by[1,2]

$$g(\mathbf{M}, \mathbf{P}) = [-4 + (1+\eta)^3 (3 + \mathbf{M} \cdot \mathbf{P}/M_s^2)/4\eta^{3/2}]^{-1}, \quad (4)$$

where η is the spin polarization constant, $\mathbf{M}$ and $\mathbf{P}$ are the magnetizations of free and fixed layers in Figure 1(b), the angle between $\mathbf{M}$ and $\mathbf{P}$ is θ. $\mathbf{M} \cdot \mathbf{P}/M_s^2 = \cos\theta$. $\mathbf{H}_{\text{STT}}$ is the corresponding effective field given by

$$\mathbf{H}_{STT} = 2\mu_B J g(\mathbf{M}, \mathbf{P}) \mathbf{M} \times \mathbf{P}/(\gamma e d M_s^3), \quad (5)$$

where μ_B, J, d, e, and M_s, are the Bohr magneton, current density, thickness of the free layer, electron charge, and saturation magnetization, respectively.

The magnetic parameters employed in the simulations are as follows: saturation magnetization $M_s = 9.549 \times 10^5$ A/m,[41] Gilbert damping parameter $\alpha = 0.00439$,[42] spin polarization factor $\eta = 0.5$,[43] magnetocrystalline anisotropy constants $K_1 = 1.2 \times 10^4$ J/m^3 and $K_2 = 0$,[35] elastic constants $c_{11} = 2.57 \times 10^{11}$ Nm^{-2}, $c_{12} = 1.62 \times 10^{11}$ Nm^{-2}, and $c_{44} = 1.05 \times 10^{11}$ Nm^{-2},[35] magnetostrictive constants $\lambda_{100} = 139ppm$ and $\lambda_{111} = 22ppm$.[41] We investigate the influence of normal substrate strain ε_{11} and ε_{22} on the magnetization state by assuming a zero shear strain. The dynamics of magnetization was investigated by numerically solving the time-dependent LLGS equation using the Gauss-Seidel projection method and the semi-implicit Fourier spectral method.[44,45] The samples were discretized in computational cells of $2 \times 2 \times 2$ nm^3, and the total size is $80 \times 80 \times 20$ nm^3.[46]

Figure 2(a) shows the temporal evolutions of magnetization components at the current density of 5.0×10^6 A/cm^2. Three lines represent magnetization component $\langle m_x \rangle$ evolutions with different substrate biaxial strains ($\varepsilon_{11} = \varepsilon_{22} = 0$,

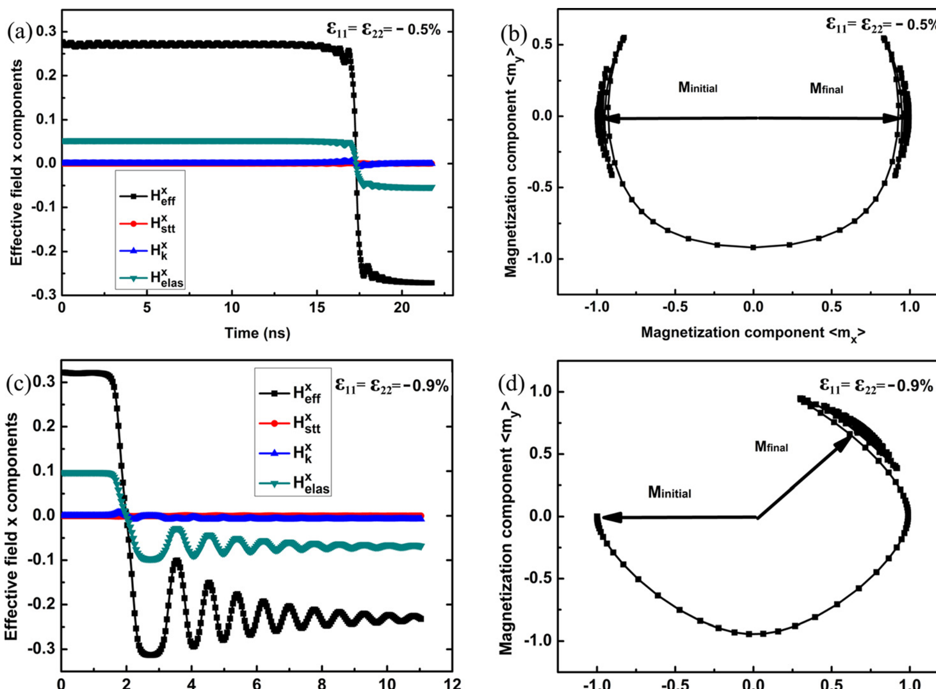

FIG. 3. (a) and (c) Temporal evolutions of effective fields along x axis at the substrate strains of −0.5% and −0.9%. (b) and (d) The magnetization trajectories projection on x-y plane at the strains of −0.5% and −0.9%.

This article is copyrighted as indicated in the article. Reuse of AIP content is subject to the terms at: http://scitation.aip.org/termsconditions. Downloaded to IP: 128.118.37.128 On: Thu, 05 Feb 2015 18:52:17

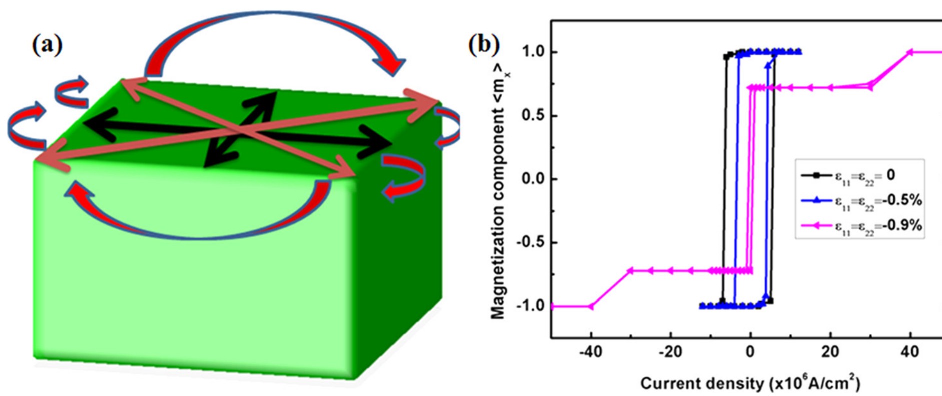

FIG. 4. (a) Schematics of strain-assisted spin transfer switching process at strain −0.9% and (b) substrate strain dependence of magnetization component $\langle m_x \rangle$ versus current density curves.

−0.5%, −0.9%). At the low current density of 5.0×10^6 A/cm^2, the magnetization cannot be switched by the spin transfer torque without substrate misfit strain. However, the magnetization switching (180° switching) can be achieved with the assistance of substrate misfit strain −0.5%. In addition, the magnetization component $\langle m_x \rangle$ will switch from −1.0 to 0.702 at the substrate biaxial strain −0.9%, which we call 135° switching. The substrate misfit strain reduces effectively the critical current and the magnetization switching time. We show the magnetization precession trajectories with zero, −0.5% and −0.9% strains at the current density of 5.0×10^6 A/cm^2. It is observed that three types of trajectories in Figure 2(b) show no switching, 180° switching, and 135° switching at zero, −0.5%, and −0.9%, respectively. The evolution of magnetic microstructure is illustrated in Figure 2(c) with the numbers corresponding to those in Figure 2(a). The 180° magnetization switching can be accomplished under the substrate strain of −0.5% (ε_{11}, ε_{22}), while the 135° magnetization switching is obtained at a higher substrate compressive strain of −0.9%. As shown in Figure 3, we show the evolutions of effective fields along x axis and the projection of magnetization trajectories on x-y plane at the biaxial substrate strains of −0.5% and −0.9%. The elastic effective field plays a significant role during the magnetization switching from AP to P. With the assistance of elastic effective field, the magnetization switching is easily accomplished by a small current input since the elastic effective field will drag the magnetization to the diagonal directions. However, the large elastic effective field will impede the 180° magnetization switching. A small current input cannot overcome the barrier of the elastic effective field, therefore, the 135° magnetization switching is obtained at the large biaxial substrate strain −0.9%. In the following, we focus on the 135° magnetization switching to achieve the strain-assisted four-state magnetization switching.

We use Figure 4(a) to illustrate the process of strain-assisted spin transfer switching. Three-step magnetization switching has four resistance states that are useful in designing multi-bit MRAM. Figure 4(b) shows the hysteresis loops at different substrate strains ($\varepsilon_{11} = \varepsilon_{22} = 0$, −0.5%, −0.9%). At the biaxial strain −0.5%, we observe the decrease of critical current for magnetization switching (blue hysteresis loop). For the strain −0.9%, we observe two intermediate states (45° and 135°) at a low current density. If we continue to increase the current density, AP and P structures can be obtained at larger positive and negative current densities, respectively. Compared with previous multilevel bit spin transfer switching,[16,28] our results have several advantages. First, it may reduce the cost of magnetic devices because only one free layer is required during the design of multilevel bit spin transfer switching magnetic devices, while two soft layers (one is hard layer and the other is soft layer) are needed in previous multilevel bit spin transfer switching devices. Second, certain transitions are prohibited in the previous structures since the hard soft layer requires a large current to switch and the soft layer can be switched by a small current. For example, “11,” “10,” “01,” and “00” in Ref. 16 are four resistance states, where the first digit refers to the hard soft layer. Level 00 cannot be switched into 10 state by using a single current. Only reversible transitions between 11 and 10, 01, and 00 can be achieved. However, all transitions among 0°, 45°, 135°, and 180° states can be obtained by adjusting the substrate strain. Third, the substrate strain can be produced by a piezoelectric substrate, and hence one can use voltage or electrical field to control the magnitude of strain through the converse piezoelectric effect. Despite these promising impacts, there are issues remain to be solved before the practical applications of such strain-assisted multi-bit MRAM. For example, as the memory states along the diagonal axes are essentially stabilized by biaxial strains, the possible strain relaxation may somewhat affect the long timescale device operation.

In conclusion, we investigated strain-assisted spin transfer switching in CoFeB-based magnetic tunnel junctions by combining phase field simulations with micromagnetic simulations. An effective method of strain-assisted spin transfer magnetization switching is proposed to reorient the magnetization instead of using an external magnetic field. The critical current of spin transfer switching is shown to decrease with substrate biaxial strain. A potential strain-assistance multilevel bit spin transfer magnetization switching was proposed.

This work was sponsored by the US National Science Foundation under the Grant No. DMR-1410714, and by the National Science Foundation of China (No. 11174030). The computer simulations were carried out on the LION and Cyberstar clusters at the Pennsylvania State University.

[1]L. Berger, Phys. Rev. B **54**(13), 9353 (1996).
[2]J. C. Slonczewski, J. Magn. Magn. Mater. **159**(1–2), L1 (1996).
[3]J. A. Katine, F. J. Albert, R. A. Buhrman, E. B. Myers, and D. C. Ralph, Phys. Rev. Lett. **84**(14), 3149 (2000).

This article is copyrighted as indicated in the article. Reuse of AIP content is subject to the terms at: http://scitation.aip.org/termsconditions. Downloaded to IP: 128.118.37.128 On: Thu, 05 Feb 2015 18:52:17

[4]B. Özyilmaz, A. Kent, D. Monsma, J. Sun, M. Rooks, and R. Koch, Phys. Rev. Lett. **91**(6), 067203 (2003).
[5]S. I. Kiselev, J. C. Sankey, I. N. Krivorotov, N. C. Emley, R. J. Schoelkopf, R. A. Buhrman, and D. C. Ralph, Nature **425**(6956), 380 (2003).
[6]W. Rippard, M. Pufall, S. Kaka, S. Russek, and T. Silva, Phys. Rev. Lett. **92**(2), 027201 (2004).
[7]B. Ozyilmaz and A. D. Kent, Appl. Phys. Lett. **88**(16), 162506 (2006).
[8]K. Machida, N. Funabashi, K.-I. Aoshima, Y. Miyamoto, N. Kawamura, K. Kuga, and N. Shimidzu, J. Appl. Phys. **103**(7), 07A713 (2008).
[9]K. Yagami, A. Tulapurkar, A. Fukushima, and Y. Suzuki, Appl. Phys. Lett. **85**(23), 5634 (2004).
[10]G. D. Fuchs, I. N. Krivorotov, P. M. Braganca, N. C. Emley, A. G. F. Garcia, D. C. Ralph, and R. A. Buhrman, Appl. Phys. Lett. **86**(15), 152509 (2005).
[11]K. J. Lee, T. H. Y. Nguyen, and K. H. Shin, J. Magn. Magn. Mater. **304**(1), 102 (2006).
[12]Y. Jiang, G. H. Yu, Y. B. Wang, J. Teng, T. Ochiai, N. Tezuka, and K. Inomata, Appl. Phys. Lett. **86**(19), 192515 (2005).
[13]H. Meng, J. Wang, and J.-P. Wang, Appl. Phys. Lett. **88**(8), 082504 (2006).
[14]Y. Zhang, Z. Zhang, Y. Liu, B. Ma, and Q. Y. Jin, Appl. Phys. Lett. **90**(11), 112504 (2007).
[15]X. Li, Z. Zhang, Q. Y. Jin, and Y. Liu, Appl. Phys. Lett. **92**(12), 122502 (2008).
[16]C.-T. Yen, W.-C. Chen, D.-Y. Wang, Y.-J. Lee, C.-T. Shen, S.-Y. Yang, C.-H. Tsai, C.-C. Hung, K.-H. Shen, and M.-J. Tsai, Appl. Phys. Lett. **93**(9), 092504 (2008).
[17]K. Aoshima, N. Funabashi, K. Machida, Y. Miyamoto, K. Kuga, and N. Kawamura, J. Magn. Magn. Mater. **310**(2), 2018 (2007).
[18]N. Hase, B. S. D. C. S. Varaprasad, T. M. Nakatani, H. Sukegawa, S. Kasai, Y. K. Takahashi, T. Furubayashi, and K. Hono, J. Appl. Phys. **108**(9), 093916 (2010).
[19]H. B. Huang, X. Q. Ma, Z. H. Liu, F. Y. Meng, S. Q. Shi, and L. Q. Chen, J. Magn. Magn. Mater. **330**, 16 (2013).
[20]H. B. Huang, X. Q. Ma, Z. H. Liu, F. Y. Meng, Z. H. Xiao, P. P. Wu, S. Q. Shi, and L. Q. Chen, J. Appl. Phys. **110**(3), 033913 (2011).
[21]S. Mitani, J. Phys. D: Appl. Phys. **44**(38), 384003 (2011).
[22]H. Sukegawa, S. Kasai, T. Furubayashi, S. Mitani, and K. Inomata, Appl. Phys. Lett. **96**(4), 042508 (2010).
[23]H. Sukegawa, Z. Wen, K. Kondou, S. Kasai, S. Mitani, and K. Inomata, Appl. Phys. Lett. **100**(18), 182403 (2012).
[24]R. Sbiaa, R. Law, S. Y. H. Lua, E. L. Tan, T. Tahmasebi, C. C. Wang, and S. N. Piramanayagam, Appl. Phys. Lett. **99**(9), 092506 (2011).
[25]X. Lou, Z. Gao, D. V. Dimitrov, and M. X. Tang, Appl. Phys. Lett. **93**(24), 242502 (2008).
[26]H. B. Huang, X. Q. Ma, Z. H. Liu, C. P. Zhao, S. Q. Shi, and L. Q. Chen, Appl. Phys. Lett. **102**(4), 042405 (2013).
[27]A. Hubert and R. Schäfer, *Magnetic Domains: The Analysis of Magnetic Microstructure* (Springer, Berlin, 1998).
[28]M. Johnson, P. Bloemen, F. Den Broeder, and J. De Vries, Rep. Prog. Phys. **59**(11), 1409 (1996).
[29]D. Sander, Rep. Prog. Phys. **62**(5), 809 (1999).
[30]K. Ahn, T. Lookman, and A. Bishop, Nature **428**(6981), 401 (2004).
[31]A. Mukherjee, W. S. Cole, P. Woodward, M. Randeria, and N. Trivedi, Phys. Rev. Lett. **110**(15), 157201 (2013).
[32]N. A. Pertsev, Phys. Rev. B **78**(21), 212102 (2008).
[33]J. Wang, J.-M. Hu, L.-Q. Chen, and C.-W. Nan, Appl. Phys. Lett. **103**(14), 142413 (2013).
[34]J.-M. Hu and C. W. Nan, Phys. Rev. B **80**(22), 224416 (2009).
[35]N. A. Pertsev and H. Kohlstedt, Adv. Funct. Mater. **22**(22), 4696 (2012).
[36]J. X. Zhang and L. Q. Chen, Philos. Mag. Lett. **85**(10), 533 (2005).
[37]H. Huang, X. Ma, Z. Liu, C. Zhao, and L. Chen, AIP Adv. **3**(3), 032132 (2013).
[38]H. Huang, X. Ma, T. Yue, Z. Xiao, S. Shi, and L. Chen, Sci. China Phys. Mech. Astron. **54**(7), 1227 (2011).
[39]M. E. Schabes and A. Aharoni, IEEE Trans. Magn. **23**(6), 3882 (1987).
[40]J.-M. Hu, T. N. Yang, L. Q. Chen, and C. W. Nan, J. Appl. Phys. **114**(16), 164303 (2013).
[41]S. Ikeda, K. Miura, H. Yamamoto, K. Mizunuma, H. Gan, M. Endo, S. Kanai, J. Hayakawa, F. Matsukura, and H. Ohno, Nature Mater. **9**(9), 721 (2010); R. C. Hall, J. Appl. Phys. **31**, S157 (1960).
[42]C. Vaz, J. Bland, and G. Lauhoff, Rep. Prog. Phys. **71**(5), 056501 (2008).
[43]J. P. Cascales, D. Herranz, J. L. Sambricio, U. Ebels, J. A. Katine, and F. G. Aliev, Appl. Phys. Lett. **102**, 092404 (2013).
[44]H. Huang, X. Ma, Z. Liu, and L. Chen, J. Alloys Compd. **597**, 230 (2014).
[45]H. Huang, X. Ma, Z. Liu, C. Zhao, and L. Chen, J. Appl. Phys. **115**(13), 133905 (2014).
[46]R. K. Tiwari, M. H. Jhon, N. Ng, D. J. Srolovitz, and C. K. Gan, Appl. Phys. Lett. **104**(2), 022413 (2014).

This article is copyrighted as indicated in the article. Reuse of AIP content is subject to the terms at: http://scitation.aip.org/termsconditions. Downloaded to IP: 128.118.37.128 On: Thu, 05 Feb 2015 18:52:17